Hindawi
Acta Neurologica Scandinavica
Volume 2023, Article ID 3012996, 11 pages
https://doi.org/10.1155/2023/3012996

Research Article

Prediction of Basal Ganglia Hematoma Expansion Based on Radiomics and Clinical Characteristics: A Novel Multivariate Predictive Nomogram

Bin Luo,[1,2] **Lin Ma**,[1] **Yubo Wang**,[1] **Hecheng Ren**,[1] **MingSheng Yu**,[1] **YuXiang Ma**,[1] **Long Yin**,[1] **and Ying Huang**[1]

[1]*Department of Neurosurgery, Tianjin Huanhu Hospital, Tianjin, China*
[2]*Academy of Medical Engineering and Translational Medicine, Tianjin University, Tianjin, China*

Correspondence should be addressed to Ying Huang; doctor_luo@tju.edu.cn

Received 30 May 2023; Revised 2 August 2023; Accepted 22 August 2023; Published 2 September 2023

Academic Editor: Nicola Tambasco

Background. This study is aimed at formulating and authenticating a pioneering nomogram integrating noncontrast computed tomography (NCCT) mean CT densities (m-CTD) of hematoma, morphological indicators from NCCT hematoma, and clinical manifestations to foresee hematoma expansion (HE) in patients suffering from spontaneous basal ganglia hemorrhage (BGH). *Methods*. A predictive model was constructed by retrospectively evaluating the data from 406 patients. This model was externally validated using an independent dataset of 174 patients. Multivariate logistic regression analysis was deployed to discern independent prognostic indicators and to generate a nomogram for HE prediction. Model calibration was examined using 1000 bootstrap samples for internal validation. *Results*. Multivariate logistic regression disclosed that m-CTD (odds ratio (OR) 0.846, 95% confidence interval (CI) 0.782-0.909), baseline hematoma volume (BHV) (OR 1.055, 95% CI 1.017-1.095), NCCT blend sign (BS) (OR 3.320, 95% CI 1.704-6.534), NCCT black hole sign (BHS) (OR 2.468, 95% CI 1.293-4.729), systolic blood pressure (SBP) (OR 1.027, 95% CI 1.014-1.040), and homocysteine (Hcy) (OR 1.075, 95% CI 1.038-1.114) were independent predictors of HE. The area under the curve (AUC) for the training and validation datasets yielded 0.874 and 0.883, respectively. The calibration curve for the nomogram closely approximated the optimal diagonal. The decision curve analysis (DCA) indicated that the prediction model offers substantial net benefits. *Conclusions*. The innovative predictive nomogram, leveraging radiomics and clinical traits of hematoma, presents a potent and noninvasive tool for HE risk stratification. The method of quantifying mean hematoma density holds significant prognostic value in forecasting HE.

1. Introduction

Despite significant advancements in the treatment of intracranial hemorrhage (ICH), it still leaves open the chance of receiving a poor prognosis [1]. Hematoma expansion (HE) which typically manifests within the initial 24 hours following cerebral hemorrhage onset is a proven prognostic indicator of subsequent neurological decline and unfavorable patient outcomes [2]. The basal ganglia, as the most frequent site of ICH, underscores the fact that even minuscule increases in HE can markedly elevate disability and mortality rates [3–5].

Contemporary research suggests that hypertension, baseline hemorrhage volume (BHV), and specific noncontrast computed tomography (NCCT) hematoma morphological indicators such as blend sign (BS), black hole sign (BHS), and island sign (IS) are effective predictors of HE [6–11]. Yet, these NCCT signs, which predict HE through qualitative analysis of hematomas, are subject to imaging-induced subjective error. Moreover, the predictive sensitivity of these individual factors for HE is modest at best (sensitivity < 30%) [12]. However, it has been suggested that quantitative analysis of hematoma density may enhance predictive accuracy, as evidenced by Barras et al. [13], who achieved considerable

predictive efficacy through quantitative NCCT hematoma density analysis.

While the computed tomography angiography (CTA) spot sign is a potent predictor of HE, its routine application in ICH diagnosis is constrained by its limited accessibility. Conversely, NCCT is ubiquitously available and retains its position as the diagnostic gold standard for ICH [14, 15]. Integrating NCCT morphological indicators with clinical risk factors can amplify the sensitivity and negative predictive value (NPV) of HE prediction [16].

Consequently, this study is aimed at constructing a HE predictive model, leveraging clinical data and NCCT markers, in a single-center cohort, with the overarching goal of bolstering the accuracy of HE identification.

2. Materials and Methods

2.1. Patient Selection. Data were compiled from patients presenting with BGH at a solitary medical center (Figure 1). The selection pool comprised 2984 patients admitted for ICH to Tianjin Huanhu Hospital from October 1, 2016, through December 31, 2022. A subset of 580 patients, with comprehensive data and meeting the defined inclusion criteria, was further selected. In a 7 : 3 random distribution, 406 patients (285 males and 121 females) were allocated to the training cohort, while 174 patients (116 males and 58 females) were assigned to the validation cohort (Figure 1). Initial NCCT and subsequent follow-up NCCT data, collected within 24 hours postsymptom onset, were retrieved for each patient. Likewise, laboratory test results conducted within this 24-hour window were also obtained. Patient management, encompassing blood pressure regulation and complication management, adhered to unified standards, following the American Heart Association/American Stroke Association guidelines for spontaneous intracerebral hemorrhage management [1].

This study obtained ethical approval from the Ethics Committee of Tianjin Huanhu Hospital and adhered to the ethical standards set forth in the 1964 Helsinki Declaration and its subsequent amendments or equivalent standards.

Inclusion criteria are as follows: (1) patient age ≥ 18 years, (2) initial NCCT scan conducted within 6 hours from the time last seen well and a subsequent NCCT conducted within 24 hours postadmission, and (3) patients experiencing their first episode.

Exclusion criteria are as follows: (1) underwent surgery prior to follow-up NCCT scan; (2) patients with cerebral hemorrhage due to head trauma, arteriovenous malformation, cerebral aneurysm, brain tumor, or venous sinus embolism; (3) spontaneous intraventricular hemorrhage; (4) concomitant subarachnoid hemorrhage; (5) hemorrhagic transformation of acute ischemic stroke; (6) baseline hematoma volume (BHV) ≤ 5 mL; and (7) antithrombotic medication prior to symptom onset.

2.2. Imaging Acquisition and Analysis. Baseline and follow-up NCCT scans were configured with a conventional 5 mm slice thickness.

Baseline and subsequent NCCT measurements were independently executed by two proficient neuroimaging physicians utilizing the ITK-SNAP software (http://www.itksnap.org). With the threshold range established at 35-100 Hounsfield units (HU), a semiautomated approach was adopted to assess all baseline hematoma volumes (BHV), the m-CTD of the hematoma, and to discern the presence or absence of BS, BHS, and IS, respectively (Figure 2). Any conflicting observations between the two investigators were arbitrated by a third party. HE was defined as either a 6 mL volume increase in hematoma or a 33% escalation from the baseline hematoma volume [17].

Images were obtained via a picture archiving and communication system and stored in Digital Imaging and Communications in Medicine (DICOM) format for subsequent review.

2.3. Definition of Mean CT Densities (m-CTD) of Hematoma. ITK-SNAP software was used to mark the hematoma in NCCT in 3D, and then, the average Hounsfield units (HU) value of the marked hematoma was automatically analyzed by the software (Figure 2(a)).

2.4. Definition of NCCT Signs. The blend sign (Figure 2(e)) denotes a comparatively hypodense area adjacent to a hyperdense area of the hematoma, with a discernible margin and a density variance of at least 18 HU between the two regions [10]. The black hole sign (Figure 2(f)) is characterized as a region of lower attenuation enveloped by a region of higher attenuation, with the attenuation disparity between the two regions exceeding 28 HU [11]. The island sign (Figure 2(g)) is distinguished by the presence of either ≥3 scattered minor hematomas, entirely segregated from the primary hematoma, or ≥4 smaller hematomas, of which some or all might be linked to the main hematoma [9].

2.5. Statistical Analysis. Statistical computations and analyses were executed utilizing the R software (version 4.2.1). All samples were arbitrarily divided into a training cohort (70%) and a validation cohort (30%) in a 7 : 3 ratio. The training cohort facilitated model construction, while the validation cohort was employed for external validation. Continuous variables conforming to a normal distribution were presented as $\bar{x} \pm s$, and Student's T test was implemented for intergroup comparisons. Alternatively, variables were denoted as median (interquartile range (IQR)), and the rank-sum test was leveraged for group comparisons. Categorical variables were represented as numbers (%), and either the chi-square test (χ^2) or Fisher's exact test was used for intergroup comparisons.

First, in the training cohort, univariate logistic regression analysis was employed to discern potential predictors of HE, and variables with $P < 0.1$ were incorporated into the multivariate logistic regression to construct the predictive model. Second, a clinical nomogram was devised to illustrate the predictive model for HE, utilizing the "rms" data package of the R software. Thereafter, the predictive efficacy of the model was evaluated by ascertaining the area under the receiver operating characteristic (ROC) curve. Calibration

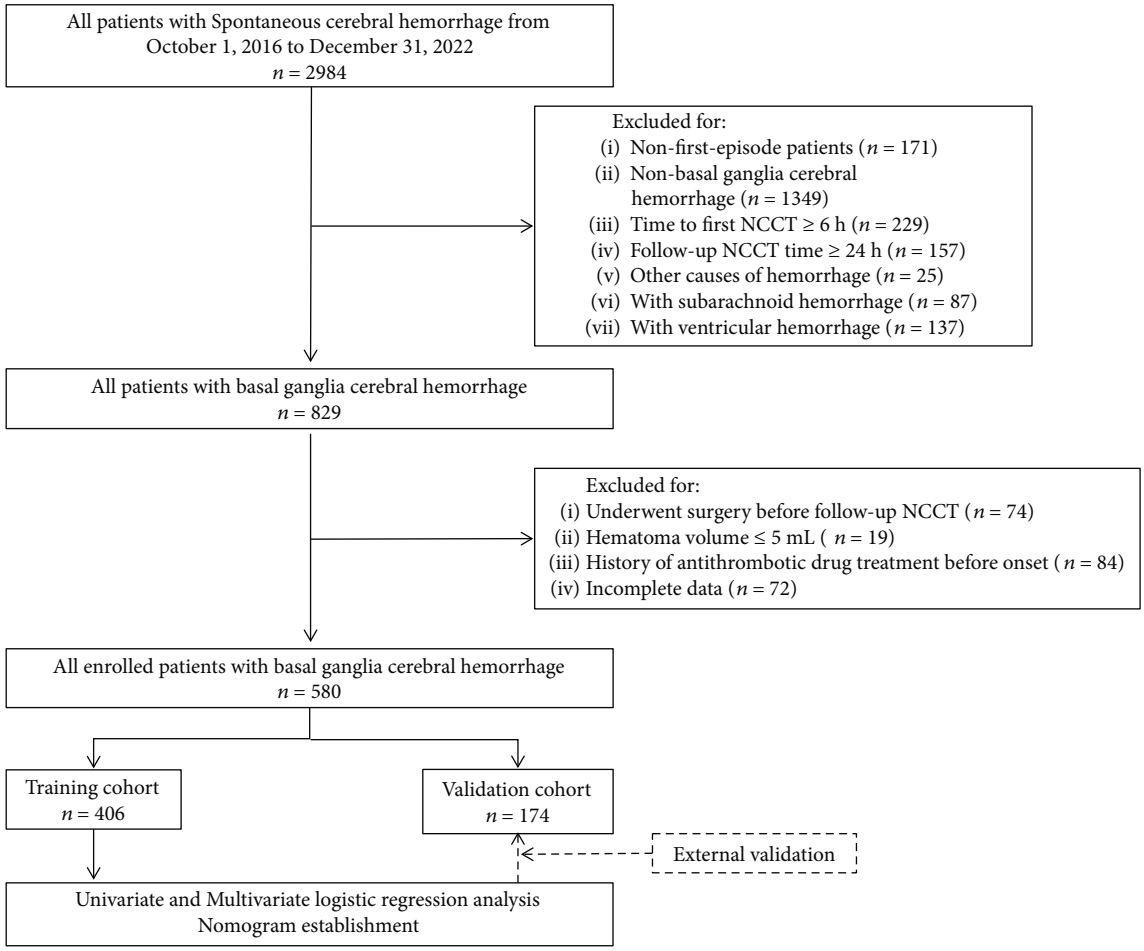

Figure 1: Patient selection flowchart. NCCT denotes noncontrast computed tomography.

curves were subsequently plotted, and 1000 internal bootstrap samples were utilized to validate the model, assessing the calibration of the predictive model. The DCA evaluated the clinical efficacy of the predictive model by determining the threshold range. Finally, the established model was further validated within the validation cohort, and the calibration curve, ROC curve, and DCA were plotted. All tests incorporated two-tailed tests. $P < 0.05$ was considered to be statistically significant.

3. Results

3.1. Baseline Characteristics. The study included a total of 580 patients diagnosed with spontaneous BGH, of whom 167 instances (28.79%) developed HE. Of the 406 patients allocated to the training cohort, 117 (28.82%) manifested HE, while 50 (28.74%) of the 174 patients in the validation cohort exhibited the same. No significant disparities were detected in the statistical comparisons between the two cohorts (Table 1).

The comparison of the non-HE and HE groups in the training cohort revealed significant discrepancies in m-CTD of hematoma ($P < 0.001$), BHV ($P < 0.001$), BS ($P < 0.001$), BHS ($P = 0.002$), SBP ($P < 0.001$), DBP ($P < 0.001$), hemoglobin ($P = 0.002$), and Hcy ($P < 0.001$) (Table 2).

3.2. Independent Predictors of HE. Independent predictors of HE were identified through multivariate logistic regression analysis. The results indicated that m-CTD of hematoma (odds ratio (OR) 0.846, 95% confidence interval (CI) 0.782-0.909, $P < 0.001$), BHV (OR 1.055, 95% CI 1.017-1.095, $P = 0.005$), BS (OR 3.320, 95% CI 1.704-6.534, $P < 0.001$), BHS (OR 2.468, 95% CI 1.293-4.729, $P = 0.006$), age (OR 1.015, 95% CI 0.996-1.035, $P = 0.116$), SBP (OR 1.027, 95% CI 1.014-1.040, $P < 0.001$), hemoglobin (OR 1.012, 95% CI 0.998-1.026, $P = 0.084$), and Hcy (OR 1.075, 95% CI 1.038-1.114, $P < 0.001$) were selected as salient components for the final prediction model (Table 3).

3.3. Construction of the Predictive Nomogram and Preliminary Validation. Drawing upon the identified predictors for HE, a nomogram was constructed (Figure 3(a)). The receiver operating characteristic (ROC) curve of the training cohort substantiated the discriminating ability of the prediction model (AUC = 0.874, 95% CI 0.835–0.912) (Figure 3(c)). The decision analysis curve (DAC) of the training cohort showed the nomogram's strong predictive performance within a risk

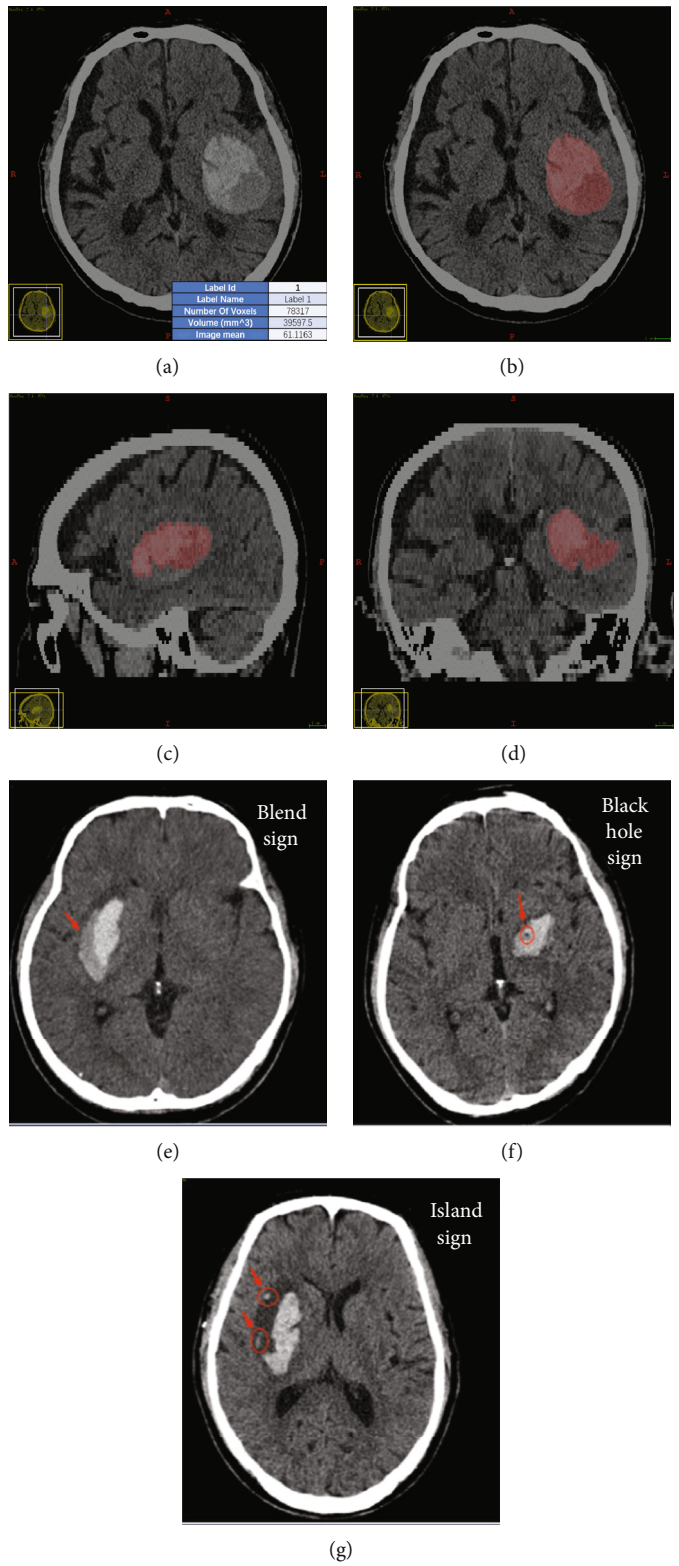

FIGURE 2: Semiautomatic ITK-SNAP measurement of hematoma volume and m-CTD (a). The red areas depict the region of interest (ROI) of the hematoma in the cross-sectional, sagittal, and coronal sections, respectively (b–d). (e–g) Schematics of the blend sign, black hole sign, and island sign, respectively. ROI = region of interest; m-CTD = mean CT densities.

Table 1: Baseline characteristics of all patients.

Variables	Total $n = 580$	Training cohort $n = 406$	Validation cohort $n = 174$	P
m-CTD of hematoma (Hu)	65.24 (62.43, 68.24)	65.00 (62.37, 68.24)	65.63 (62.57, 68.16)	0.534
BHV (mL)	13.35 (7.28, 20.62)	13.94 (7.53, 21.31)	12.40 (6.84, 19.42)	0.174
BS				0.225
No	478 (82.41%)	329 (81.03%)	149 (85.63%)	
Yes	102 (17.59%)	77 (18.97%)	25 (14.37%)	
BHS				0.312
No	481 (82.93%)	332 (81.77%)	149 (85.63%)	
Yes	99 (17.07%)	74 (18.23%)	25 (14.37%)	
IS				0.525
No	568 (97.93%)	396 (97.54%)	172 (98.85%)	
Yes	12 (2.07%)	10 (2.46%)	2 (1.15%)	
HE				1.000
No	413 (71.21%)	289 (71.18%)	124 (71.26%)	
Yes	167 (28.79%)	117 (28.82%)	50 (28.74%)	
Gender				0.456
F	179 (30.86%)	121 (29.80%)	58 (33.33%)	
M	401 (69.14%)	285 (70.20%)	116 (66.67%)	
Age (years)	56.00 (47.00, 67.00)	56.00 (47.00, 67.00)	56.00 (46.00, 65.00)	0.438
SBP (mmHg)	165.15 ± 22.69	165.02 ± 23.18	165.45 ± 21.56	0.828
DBP (mmHg)	95.00 (87.00, 104.00)	95.00 (86.75, 104.00)	95.00 (88.00, 104.00)	0.872
Hemoglobin (g/L)	138.00 (122.00, 154.00)	141.00 (124.00, 153.00)	134.50 (119.25, 154.00)	0.193
Platelet count ($\times 10^9$/L)	207.00 (166.00, 243.00)	209.00 (167.00, 243.00)	203.00 (157.50, 245.25)	0.331
APTT (s)	25.30 (22.70, 30.70)	25.45 (22.50, 30.80)	25.05 (23.10, 30.15)	0.831
PT (s)	11.70 (10.88, 12.70)	11.80 (10.83, 12.80)	11.60 (10.90, 12.60)	0.909
TT (s)	17.10 (16.10, 18.20)	17.10 (16.10, 18.20)	17.10 (16.10, 18.10)	0.912
FIB (g/L)	2.96 (2.18, 4.22)	2.96 (2.17, 4.36)	2.95 (2.18, 4.03)	0.962
INR (s)	0.98 (0.85, 1.14)	0.98 (0.85, 1.13)	0.99 (0.86, 1.17)	0.416
Blood glucose (mmol/L)	8.71 (6.08, 12.07)	8.71 (6.18, 12.03)	8.71 (5.50, 12.18)	0.484
Total cholesterol (mmol/L)	4.34 (3.28, 5.49)	4.30 (3.23, 5.50)	4.40 (3.38, 5.46)	0.510
Triglycerides (mmol/L)	1.26 (0.77, 1.74)	1.24 (0.75, 1.77)	1.30 (0.80, 1.71)	0.968
Hcy (μmol/L)	13.85 (9.65, 18.28)	14.09 (9.51, 18.63)	13.71 (9.68, 18.16)	0.807

Data are expressed as n (%), $\bar{x} \pm s$, or median (interquartile range (IQR)). $P < 0.05$ was considered to be statistically significant. IQR = interquartile range; m-CTD = mean CT densities; BHV = baseline hemorrhage volume; BS = blend sign; BHS = basal ganglia hemorrhage; IS = island sign; HE = hematoma expansion; SBP = systolic blood pressure; DBP = diastolic blood pressure; APTT = activated partial thromboplastin time; PT = prothrombin time; TT = thrombin time; FIB = fibrinogen; INR = international normalized ratio; Hcy = homocysteine.

threshold of 0.05–0.8, with optimal efficacy observed around a risk threshold of 0.4 (Figures 3(d) and 3(e)). Correspondingly, the ROC curve of the validation cohort confirmed the model's discriminating capability (AUC = 0.883, 95% CI 0.831-0.936) (Figure 3(f)), in alignment with the training cohort findings. The DAC of the validation cohort demonstrated predictive efficiency within the risk threshold of 0.05–0.7, again achieving optimal performance around a risk threshold of 0.4 (Figures 3(g) and 3(h)), consistent with the training cohort. ROC curve analysis indicated that m-CTD of hematoma offers moderate predictive value in both the training and validation cohorts, with the area under the ROC curve surpassing 0.7 (AUC = 0.776, 95% CI 0.725–0.827 vs. AUC = 0.730, 95% CI 0.643–0.817) (Figure 3(b)).

The calibration curves for both cohorts underscored the robust alignment between predicted and actual probabilities, reflecting the high calibration of our constructed prediction model (Figures 3(d) and 3(g)).

3.4. Multivariate Analysis of the Overall Predictive Power. ROC analyses were conducted for all isolated risk factors, capturing sensitivity and specificity measures. In alignment with our hypothesis, these NCCT predictors exhibited strong predictive performance. The multivariate predictive power of the m-CTD in conjunction with other radiomics and clinical characteristics surpassed the accuracy of single-factor prediction (AUC 0.865, sensitivity 0.749, and specificity 0.860). Cut-off values for these factors were determined as follows:

Table 2: Baseline characteristics of patients with and without HE.

Variables	Training cohort		P
	Non-HE ($n = 289$)	HE ($n = 117$)	
m-CTD of hematoma (Hu)	66.49 (63.83, 68.73)	62.25 (60.35, 64.35)	<0.001
BHV (mL)	11.77 (6.52, 17.24)	20.76 (13.23, 25.16)	<0.001
BS			<0.001
No	260 (89.97%)	69 (58.97%)	
Yes	29 (10.03%)	48 (41.03%)	
BHS			0.002
No	248 (85.81%)	84 (71.79%)	
Yes	41 (14.19%)	33 (28.21%)	
IS			>0.99
No	282 (97.58%)	114 (97.44%)	
Yes	7 (2.42%)	3 (2.56%)	
Gender			0.198
F	92 (31.83%)	29 (24.79%)	
M	197 (68.17%)	88 (75.21%)	
Age (years)	56.00 (47.00, 66.00)	57.00 (51.00, 69.00)	0.069
SBP (mmHg)	159.00 (145.00, 175.00)	185.00 (162.00, 194.00)	<0.001
DBP (mmHg)	94.00 (86.00, 100.00)	100.00 (93.00, 108.00)	<0.001
Hemoglobin (g/L)	136.00 (123.00, 150.00)	149.00 (127.00, 157.00)	0.002
Platelet count ($\times 10^9$/L)	210.00 (168.00, 241.00)	207.00 (166.00, 247.00)	0.924
APTT (s)	25.50 (22.50, 30.80)	25.10 (22.70, 30.80)	0.612
PT (s)	11.70 (10.80, 12.70)	11.80 (10.90, 13.10)	0.405
TT (s)	17.10 (16.00, 18.20)	17.30 (16.40, 18.30)	0.254
FIB (g/L)	3.01 (2.19, 4.35)	2.84 (2.12, 4.38)	0.742
INR (s)	0.99 (0.86, 1.15)	0.96 (0.81, 1.09)	0.206
Blood glucose (mmol/L)	8.79 (6.16, 12.18)	8.49 (6.18, 11.74)	0.868
Total cholesterol (mmol/L)	4.28 (3.28, 5.49)	4.37 (3.14, 5.52)	0.943
Triglycerides (mmol/L)	1.24 (0.76, 1.75)	1.19 (0.75, 1.83)	0.889
Hcy (μmol/L)	12.46 (8.25, 16.30)	17.88 (13.93, 21.48)	<0.001

Data are expressed as n (%) or median (IQR). $P < 0.05$ was considered to be statistically significant. IQR = interquartile range; HE = hematoma expansion; Non-HE = nonhematoma expansion; m-CTD = mean CT densities; BHV = baseline hemorrhage volume; BS = blend sign; BHS = basal ganglia hemorrhage; IS = island sign; SBP = systolic blood pressure; DBP = diastolic blood pressure; APTT = activated partial thromboplastin time; PT = prothrombin time; TT = thrombin time; FIB = fibrinogen; INR = international normalized ratio; Hcy = homocysteine.

m-CTD (63.45), BHV (17.33), Hcy (14.09), and systolic pressure (181.50), respectively (Table 4 and Figure 4).

4. Discussion

HE predominantly occurs within the initial six hours following intracerebral hemorrhage (ICH) onset [17–19]. Accordingly, we utilized baseline NCCT data, procured within six hours post the latest well-observed time, to gauge the m-CTD of the hematoma and assess the radiomic features. Concurrently, the follow-up NCCT within the initial 24 hours of admission was examined to delineate between HE and non-HE cases. Our findings confirmed that m-CTD is an independent risk factor for HE prediction ($P < 0.001$), corroborating previous studies [20, 21]. When amalgamated with other factors, the predictive accuracy was enhanced, underscoring m-CTD's ability to independently anticipate HE occurrence and, when utilized as a contributing factor, augmenting the precision of the predictive model. This simple method of measuring hematoma average density can be pragmatically applied by clinicians to fortify ICH diagnosis and treatment strategies.

Variations in hematoma CT densities are profoundly associated with factors such as onset time and hematoma volume [14, 19]. Areas of hypodensity within the hematoma often indicate an elevated incidence of HE [6, 10, 11]. Paradoxically, in our clinical observations, we noted that homogeneous hematomas devoid of hypodense regions were also susceptible to HE, generally exhibiting lower density values. Conversely, certain hematomas with density heterogeneity did not progress to the anticipated HE. Numerous investigations have probed the utility of NCCT in forecasting HE [6, 10, 11, 13, 22–28], primarily focusing on qualitative or categorical designation of hematoma density regions. It is critical to acknowledge that hematoma density is not uniformly distributed and comprises various densities. We carried out a

Table 3: Univariate and multivariate logistic regression analyses identifying predictors for HE.

Variables	Univariate logistic regression		Multivariate logistic regression	
	OR (95% CI)	*P*	OR (95% CI)	*P*
m-CTD of hematoma (Hu)	0.776 (0.723, 0.828)	<0.001	0.846 (0.782, 0.909)	<0.001
BHV	1.108 (1.075, 1.143)	<0.001	1.055 (1.017, 1.095)	0.005
BS	6.237 (3.689, 10.72)	<0.001	3.320 (1.704, 6.534)	<0.001
BHS	2.376 (1.407, 3.999)	0.001	2.468 (1.293, 4.729)	0.006
Age (years)	1.016 (1.001, 1.031)	0.033	1.015 (0.996, 1.035)	0.116
SBP (mmHg)	1.039 (1.027, 1.051)	<0.001	1.027 (1.014, 1.040)	<0.001
Hemoglobin(g/L)	1.016 (1.005, 1.028)	0.005	1.012 (0.998, 1.026)	0.084
Hcy (μmol/L)	1.096 (1.063, 1.134)	<0.001	1.075 (1.038, 1.114)	<0.001
IS	1.060 (0.225, 3.886)	0.933		
Gender	1.417 (0.878, 2.333)	0.161		
DBP (mmHg)	1.036 (1.017, 1.056)	<0.001		
Platelet count ($\times 10^9$/L)	1.000 (0.996, 1.004)	0.896		
APTT (s)	0.987 (0.946, 1.028)	0.526		
PT (s)	1.085 (0.918, 1.281)	0.337		
TT (s)	1.074 (0.93, 1.241)	0.331		
FIB (g/L)	0.99 (0.84, 1.163)	0.902		
INR (s)	0.553 (0.199, 1.499)	0.250		
Blood glucose (mmol/L)	0.986 (0.933, 1.027)	0.558		
Total cholesterol (mmol/L)	1.003 (0.857, 1.174)	0.967		
Triglycerides (mmol/L)	1.039 (0.739, 1.454)	0.825		

$P < 0.05$ was considered to be statistically significant. OR = odds ratio; 95% CI = 95% confidence interval; m-CTD = mean CT densities; BHV = baseline hemorrhage volume; BS = blend sign; BHS = basal ganglia hemorrhage; SBP = systolic blood pressure; Hcy = homocysteine; IS = island sign; DBP = diastolic blood pressure; APTT = activated partial thromboplastin time; PT = prothrombin time; TT = thrombin time; FIB = fibrinogen; INR = international normalized ratio.

quantitative analysis of hematoma CT density values, which may offer a more precise and objective representation of the overall CT density profile of the hematoma. The final results presented commendable predictive performance in both training and validation cohorts, and the prediction efficacy was further optimized through multivariate combination.

High systolic blood pressure (SBP) has been identified as an independent risk factor for HE prediction, and it also impacts the baseline hemorrhage volume (BHV) of ICH [29–32]. Indeed, BHV is not only another risk factor for HE prediction but also a critical determinant of mortality and prognosis [33, 34]. Multiple studies have validated a positive correlation between hematoma expansion and larger BHV [35–37]. Aligning with these findings, we noted a significantly higher BHV in the HE group compared to the non-HE group ($P < 0.001$). These results propose a potential strategy for reducing HE incidence through early BP intervention, especially in patients presenting with sizeable BHV and low m-CTD, specifically when BHV > cut-off value 17.33 and m-CTD < cut-off value 63.45 (Table 4).

The incidence of HE escalates with age, potentially attributable to a higher prevalence of arteriosclerosis, amyloid angiopathy, hypertension, increased BHV post-ICH, and enhanced neurovascular inflammation among the elderly [38, 39]. Conventional wisdom also attributes low hemoglobin levels to the evolution of HE [40]. However, our study found a higher hemoglobin concentration in the HE group in the training cohort compared to the non-HE group ($P = 0.002$). This may not suggest that elevated hemoglobin precipitates HE but rather hints towards a decreased platelet ratio secondary to increased hemoglobin, culminating in an amplified HE incidence. This hypothesis was corroborated in our study, wherein the HE group displayed a marginally lower platelet count compared to the non-HE group within the training cohort (M (IQR), 207.00 (166.00, 247.00) vs. 210.00 (168.00, 241.00)). However, the difference was not statistically significant.

Contrary to the findings by Suo et al., which suggested lower plasma Hcy concentrations as a risk factor for HE [41], we observed higher Hcy levels in the HE group than in the non-HE group ($P < 0.001$), corroborating Zeng et al. and Li et al.'s results [42, 43]. A plausible explanation is that high Hcy levels augment matrix metalloproteinase-9 (MMP-9) production, thereby increasing vascular endothelial cell permeability and causing cell damage. MMP-9 may also compromise the blood-brain barrier by degrading type IV collagenase, laminin, and fibronectin in the extracellular matrix and basement membrane, inducing apoptosis and, subsequently, HE. Moreover, Hcy is associated with hypertension and can provoke atherosclerosis by escalating oxidative stress, damaging elastin fibers, and increasing collagen synthesis [44]. Hence, this underscores the clinical significance of early intervention in ICH patients with high Hcy levels to mitigate HE occurrence.

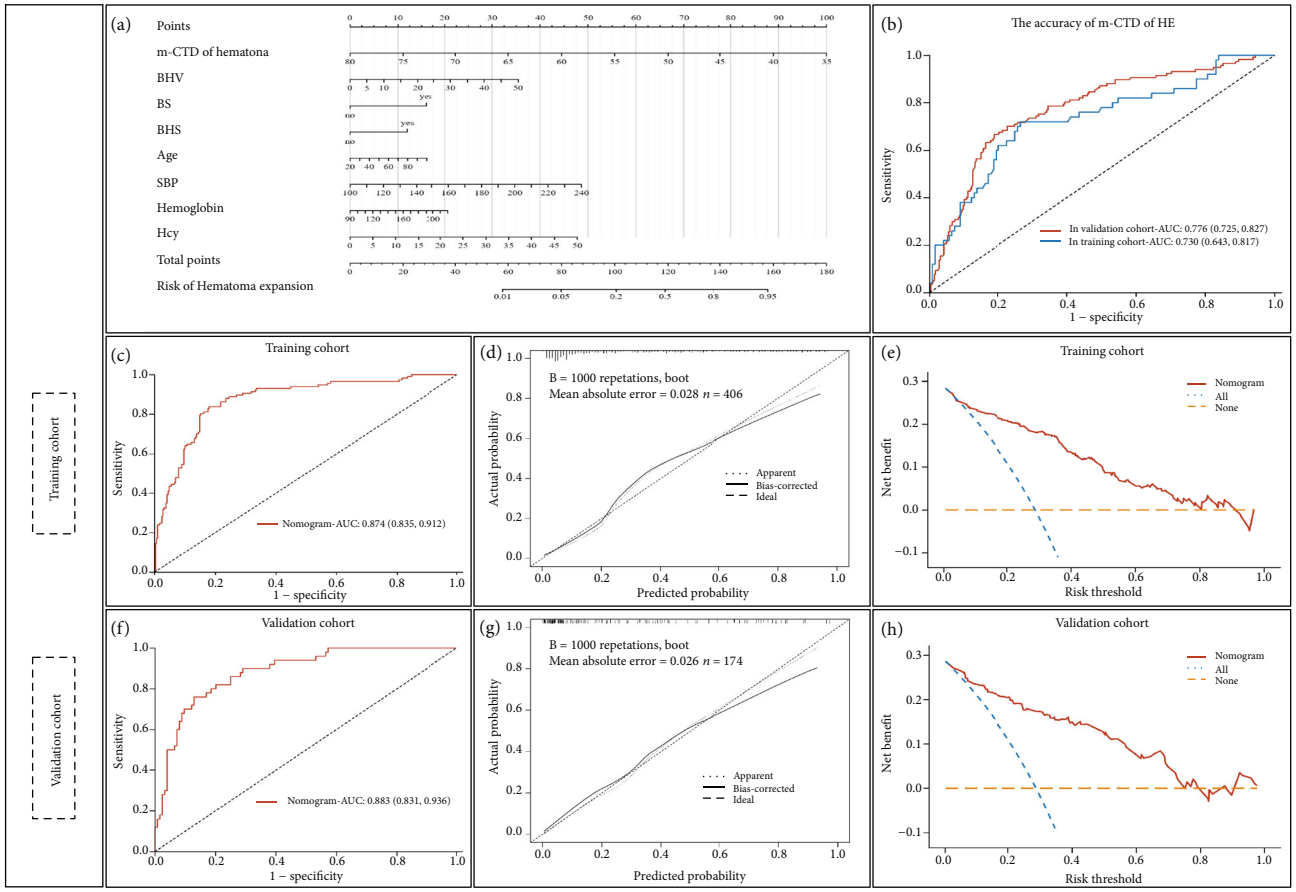

Figure 3: Constructed nomogram for predicting HE. (a) The nomogram is derived from multivariate analysis. (b) The AUCs of m-CTD in the training cohort and validation cohort were 0.776 and 0.730, respectively. (c, f) The AUCs for the training cohort and validation cohort were 0.874 and 0.883, respectively. (d, g) Calibration curves for the training and validation cohorts. (e, h) DAC curve analyses for both cohorts show the nomogram's optimal predictive efficacy at risk thresholds approximating 0.4. AUC = area under the curve; DAC = decision analysis curve; ROC = receiver operating characteristic; m-CTD = mean CT densities; BHV = baseline hemorrhage volume; BS = blend sign; BHS = basal ganglia hemorrhage; SBP = systolic blood pressure; Hcy = homocysteine.

Table 4: Comprehensive multivariate analysis of predictive power.

Variables	AUC	Sensitivity	Specificity	*P*	Cut-off value
Multivariable	0.865	0.749	0.860	<0.001	—
m-CTD (Hu)	0.762	0.653	0.804	<0.001	63.45
BHV (mL)	0.733	0.647	0.753	<0.001	17.33
Hcy (mmol/L)	0.729	0.737	0.615	<0.001	14.09
Systolic pressure (mmHg)	0.725	0.527	0.852	<0.001	181.50
Blend sign	0.646	0.383	0.908	<0.001	—
Black hole sign	0.569	0.269	0.869	0.009	—

$P < 0.05$ was considered to be statistically significant. AUC = area under the curve; m-CTD = mean CT densities; BHV = baseline hemorrhage volume; Hcy = homocysteine; SBP = systolic blood pressure; BS = blend sign; BHS = black hole sign.

5. Strengths and Limitations

The current investigation is, to our knowledge, pioneering in quantifying the m-CTD of BGH, further integrating it with CT morphological indicators and hematoma clinical characteristics to predict HE. To bolster the accuracy of our findings, we adopted stringent criteria for sample inclusion.

Nonetheless, the study has several constraints:

(1) The study's design is retrospective and confined to a single center. Therefore, prospective multicenter studies are imperative for validating these findings

(2) Given that spontaneous intracranial hemorrhages primarily occur within the basal ganglia, we did not account for thalamic or cortical bleeding, thereby introducing a selection bias. Future endeavors will

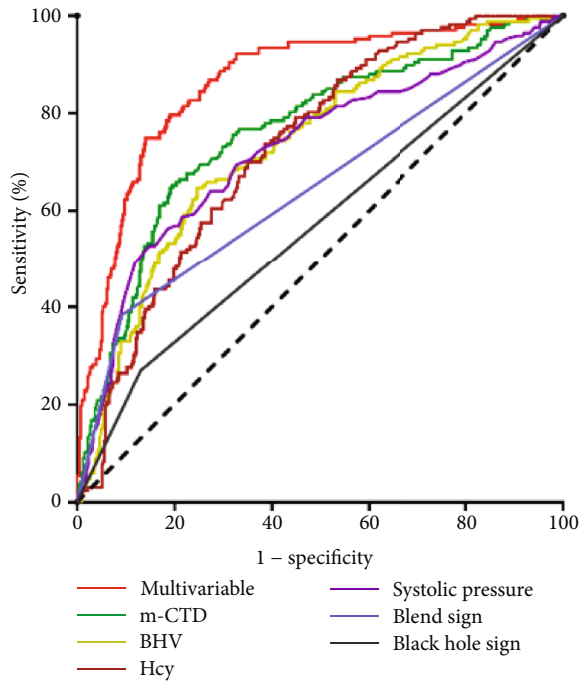

Figure 4: ROC curve analyses of the clinical and multivariable models on hematoma expansion in the training cohort and validation cohort. m-CTD = mean CT densities; BHV = baseline hemorrhage volume; Hcy = homocysteine; SBP = systolic blood pressure; BS = blend sign; BHS = black hole sign.

encompass data from these cerebral hemorrhages for a comprehensive analysis

(3) Data collection was limited to patients who underwent follow-up CT, excluding those with sizable baseline hemorrhage volumes (BHV) and those who received surgical interventions. This has inadvertently led to a dearth of data concerning HE occurrence in patients with extensive BHV

(4) We overlooked the examination timeframes of baseline NCCT and follow-up NCCT, a variable that warrants further exploration in upcoming research

6. Conclusion

The mean CT densities of hematoma, baseline hematoma volume, blend sign, black hole sign, systolic blood pressure, and homocysteine levels independently predispose patients to basal ganglia hemorrhage. Quantitative analyses of hematoma's mean CT densities significantly enhance the predictive accuracy for HE occurrence. When integrated with other risk factors, this measure notably improves comprehensive predictive capacity. Utilizing freely available, open-source ITK-SNAP software for quantifying the mean CT densities of hematoma affords a rapid, efficient method, facilitating neurologists in the diagnosis and treatment of ICH.

Abbreviations

APTT: Activated partial thromboplastin time
AUC: Area under the curve
BGH: Spontaneous basal ganglia hemorrhage.
BHS: Black hole sign
BHV: Baseline hemorrhage volume
BS: Blend sign
CI: Confidence interval
CTA: Computed tomography angiography
DAC: Decision analysis curve
DBP: Diastolic blood pressure
DICOM: Digital Imaging and Communications in Medicine
FIB: Fibrinogen
Hcy: Homocysteine
HE: Hematoma expansion
HU: Hounsfield units
INR: International normalized ratio
IQR: Interquartile range
IS: Island sign
m-CTD: Mean CT densities
NCCT: Noncontrast computed tomography
NPV: Negative predictive value
PT: Prothrombin time
ROC: Receiver operating characteristic
SBP: Systolic blood pressure
TT: Thrombin time.

Data Availability

The raw data supporting the conclusions of this article will be made available by the authors, without undue reservation. Please contact the authors if needed, and we will make the study data publicly available for further research.

Additional Points

Code Availability. The analysis code supporting the results of this study has been uploaded to the supplementary file. And the materials remain accessible for permanently.

Ethical Approval

In this study, all protocols were approved by the Institutional Review Board of Tianjin Huanhu Hospital and conducted in accordance with the 1964 Helsinki Declaration and its later amendments or comparable ethical standards. The Tianjin Huanhu Hospital Ethics Committee approved the data collection procedures that involved the study participants to ensure that they are conducted in accordance with the ethical standards.

Consent

Written informed consent for participation was not required for this study in accordance with the national legislation and the institutional requirements. Verbal informed consent was obtained prior to the interview. Written informed consent for publication was obtained from all participants.

Conflicts of Interest

The authors declare that they have no conflict of interest.

Authors' Contributions

Bin Luo, Lin Ma, YuBo Wang, HeCheng Ren, and Ying Huang were responsible for the study concept and design. Bin Luo, Lin Ma, MingSheng Yu, and YuXiang Ma were responsible for the data acquisition. Bin Luo, Lin Ma, MingSheng Yu, and YuXiang Ma were responsible for the statistical analysis. Bin Luo, Lin Ma, MingSheng Yu, and YuXiang Ma were responsible for the interpretation of data. Bin Luo, Long Yin, and Ying Huang were responsible for the manuscript drafting. Bin Luo and Ying Huang were responsible for the review and editing. Ying Huang was responsible for the supervision. All authors commented on previous versions of the manuscript. All authors read and approved the final manuscript and approved the submission to this journal. Bin Luo, Lin Ma and Yubo Wang have contributed equally to this work and share first authorship.

References

[1] S. M. Greenberg, W. C. Ziai, C. Cordonnier et al., "2022 Guideline for the management of patients with spontaneous intracerebral hemorrhage: a guideline from the American Heart Association/American Stroke Association," *Stroke*, vol. 53, no. 7, pp. e282–e361, 2022.

[2] Q. Li, A. D. Warren, A. I. Qureshi et al., "Ultra-early blood pressure reduction attenuates hematoma growth and improves outcome in intracerebral hemorrhage," *Annals of Neurology*, vol. 88, no. 2, pp. 388–395, 2020.

[3] G. Xu, M. Ma, X. Liu, and G. J. Hankey, "Is there a stroke belt in China and why?," *Stroke*, vol. 44, no. 7, pp. 1775–1783, 2013.

[4] N. Samarasekera, A. Fonville, C. Lerpiniere et al., "Influence of intracerebral hemorrhage location on incidence, characteristics, and outcome: population-based study," *Stroke*, vol. 46, no. 2, pp. 361–368, 2015.

[5] C. J. van Asch, M. J. Luitse, G. J. Rinkel, I. van der Tweel, A. Algra, and C. J. Klijn, "Incidence, case fatality, and functional outcome of intracerebral haemorrhage over time, according to age, sex, and ethnic origin: a systematic review and meta-analysis," *Lancet Neurology*, vol. 9, no. 2, pp. 167–176, 2010.

[6] G. Boulouis, A. Morotti, H. B. Brouwers et al., "Association between hypodensities detected by computed tomography and hematoma expansion in patients with intracerebral hemorrhage," *JAMA Neurology*, vol. 73, no. 8, pp. 961–968, 2016.

[7] A. Morotti, G. Boulouis, J. M. Romero et al., "Blood pressure reduction and noncontrast CT markers of intracerebral hemorrhage expansion," *Neurology*, vol. 89, no. 6, pp. 548–554, 2017.

[8] A. Morotti, D. Dowlatshahi, G. Boulouis et al., "Predicting intracerebral hemorrhage expansion with noncontrast computed tomography," *Stroke*, vol. 49, no. 5, pp. 1163–1169, 2018.

[9] Q. Li, Q. J. Liu, W. S. Yang et al., "Island sign," *Stroke*, vol. 48, no. 11, pp. 3019–3025, 2017.

[10] Q. Li, G. Zhang, Y. J. Huang et al., "Blend sign on computed tomography," *Stroke*, vol. 46, no. 8, pp. 2119–2123, 2015.

[11] Q. Li, G. Zhang, X. Xiong et al., "Black hole sign," *Stroke*, vol. 47, no. 7, pp. 1777–1781, 2016.

[12] D. Zhang, J. Chen, Q. Xue et al., "Heterogeneity signs on noncontrast computed tomography predict hematoma expansion after intracerebral hemorrhage: a meta-analysis," *BioMed Research International*, vol. 2018, Article ID 6038193, 9 pages, 2018.

[13] C. D. Barras, B. M. Tress, S. Christensen et al., "Quantitative CT densitometry for predicting intracerebral hemorrhage growth," *American Journal of Neuroradiology*, vol. 34, no. 6, pp. 1139–1144, 2013.

[14] A. M. Demchuk, D. Dowlatshahi, D. Rodriguez-Luna et al., "Prediction of haematoma growth and outcome in patients with intracerebral haemorrhage using the CT-angiography spot sign (PREDICT): a prospective observational study," *Lancet Neurology*, vol. 11, no. 4, pp. 307–314, 2012.

[15] A. Morotti, H. B. Brouwers, J. M. Romero et al., "Intensive blood pressure reduction and spot sign in intracerebral hemorrhage," *JAMA Neurology*, vol. 74, no. 8, pp. 950–960, 2017.

[16] Q. Chen, D. Zhu, J. Liu et al., "Clinical-radiomics nomogram for risk estimation of early hematoma expansion after acute intracerebral hemorrhage," *Academic Radiology*, vol. 28, no. 3, pp. 307–317, 2021.

[17] D. Dowlatshahi, A. M. Demchuk, M. L. Flaherty et al., "Defining hematoma expansion in intracerebral hemorrhage: relationship with patient outcomes," *Neurology*, vol. 76, no. 14, pp. 1238–1244, 2011.

[18] J. M. Romero, H. B. Brouwers, J. Lu et al., "Prospective validation of the computed tomographic angiography spot sign score for intracerebral hemorrhage," *Stroke*, vol. 44, no. 11, pp. 3097–3102, 2013.

[19] K. Toyoda, Y. Okada, K. Minematsu et al., "Antiplatelet therapy contributes to acute deterioration of intracerebral hemorrhage," *Neurology*, vol. 65, no. 7, pp. 1000–1004, 2005.

[20] H. G. Jeong, J. S. Bang, B. J. Kim, H. J. Bae, and M. K. Han, "Hematoma Hounsfield units and expansion of intracerebral hemorrhage: a potential marker of hemostatic clot contraction," *International Journal of Stroke*, vol. 16, no. 2, pp. 163–171, 2021.

[21] Y. Chen, D. Cao, Z. Q. Guo et al., "The attenuation value within the non-hypodense region on non-contrast computed tomography of spontaneous cerebral hemorrhage: a long-neglected predictor of hematoma expansion," *Frontiers in Neurology*, vol. 13, article 785670, 2022.

[22] S. Kazui, H. Naritomi, H. Yamamoto, T. Sawada, and T. Yamaguchi, "Enlargement of spontaneous intracerebral hemorrhage: incidence and time course," *Stroke*, vol. 27, no. 10, pp. 1783–1787, 1996.

[23] D. Blacquiere, A. M. Demchuk, M. Al-Hazzaa et al., "Intracerebral hematoma morphologic appearance on noncontrast computed tomography predicts significant hematoma expansion," *Stroke*, vol. 46, no. 11, pp. 3111–3116, 2015.

[24] X. Yao, Y. Xu, E. Siwila-Sackman, B. Wu, and M. Selim, "The HEP score: a nomogram-derived hematoma expansion prediction scale," *Neurocritical Care*, vol. 23, no. 2, pp. 179–187, 2015.

[25] S. Chan, C. Conell, K. T. Veerina, V. A. Rao, and A. C. Flint, "Prediction of intracerebral haemorrhage expansion with clinical, laboratory, pharmacologic, and noncontrast radiographic

variables," *International Journal of Stroke*, vol. 10, no. 7, pp. 1057–1061, 2015.

[26] J. Witsch, E. Bruce, E. Meyers et al., "Intraventricular hemorrhage expansion in patients with spontaneous intracerebral hemorrhage," *Neurology*, vol. 84, no. 10, pp. 989–994, 2015.

[27] W. Xu, H. Guo, H. Li et al., "A non-contrast computed tomography-based radiomics nomogram for the prediction of hematoma expansion in patients with deep ganglionic intracerebral hemorrhage," *Frontiers in Neurology*, vol. 13, article 974183, 2022.

[28] M. Zhang, J. Chen, C. Zhan et al., "Blend sign is a strong predictor of the extent of early hematoma expansion in spontaneous intracerebral hemorrhage," *Frontiers in Neurology*, vol. 11, p. 334, 2020.

[29] A. I. Qureshi, W. Huang, I. Lobanova et al., "Outcomes of intensive systolic blood pressure reduction in patients with intracerebral hemorrhage and excessively high initial systolic blood pressure: post hoc analysis of a randomized clinical trial," *JAMA Neurology*, vol. 77, no. 11, pp. 1355–1365, 2020.

[30] L. B. Morgenstern, J. C. Hemphill 3rd, C. Anderson et al., "Guidelines for the management of spontaneous intracerebral hemorrhage: a guideline for healthcare professionals from the American Heart Association/American Stroke Association," *Stroke*, vol. 41, no. 9, pp. 2108–2129, 2010.

[31] W. Li, C. Jin, A. Vaidya et al., "Blood Pressure Trajectories and the Risk of Intracerebral Hemorrhage and Cerebral Infarction: A Prospective Study," *Hypertension*, vol. 70, no. 3, pp. 508–514, 2017.

[32] D. M. Oh, K. Shkirkova, R. A. Poblete et al., "Association between hyperacute blood pressure variability and hematoma expansion after intracerebral hemorrhage: secondary analysis of the FAST-MAG database," *Neurocritical Care*, vol. 38, no. 2, pp. 356–364, 2023.

[33] R. Al-Shahi Salman, Z. K. Law, P. M. Bath, T. Steiner, and N. Sprigg, "Haemostatic therapies for acute spontaneous intracerebral haemorrhage," *The Cochrane Database of Systematic Reviews*, vol. 4, article Cd005951, 2018.

[34] A. Hillal, T. Ullberg, B. Ramgren, and J. Wassélius, "Computed tomography in acute intracerebral hemorrhage: neuroimaging predictors of hematoma expansion and outcome," *Insights Into Imaging*, vol. 13, no. 1, p. 180, 2022.

[35] L. R. Kuohn, J. Witsch, T. Steiner et al., "Early deterioration, hematoma expansion, and outcomes in deep versus lobar intracerebral hemorrhage: the FAST trial," *Stroke*, vol. 53, no. 8, pp. 2441–2448, 2022.

[36] A. Morotti, G. Boulouis, D. Dowlatshahi et al., "Intracerebral haemorrhage expansion: definitions, predictors, and prevention," *Lancet Neurology*, vol. 22, no. 2, pp. 159–171, 2023.

[37] L. Song, X. M. Qiu, T. T. Guo et al., "Association between anatomical location and hematoma expansion in deep intracerebral hemorrhage," *Frontiers in Neurology*, vol. 12, article 749931, 2022.

[38] Y. Béjot, C. Cordonnier, J. Durier, C. Aboa-Eboulé, O. Rouaud, and M. Giroud, "Intracerebral haemorrhage profiles are changing: results from the Dijon population-based study," *Brain*, vol. 136, no. 2, pp. 658–664, 2013.

[39] J. B. Kuramatsu, R. Sauer, C. Mauer et al., "Correlation of age and haematoma volume in patients with spontaneous lobar intracerebral haemorrhage," *Journal of Neurology, Neurosurgery, and Psychiatry*, vol. 82, no. 2, pp. 144–149, 2011.

[40] D. J. Roh, D. J. Albers, J. Magid-Bernstein et al., "Low hemoglobin and hematoma expansion after intracerebral hemorrhage," *Neurology*, vol. 93, no. 4, pp. e372–e380, 2019.

[41] Y. Suo, W. Chen, Y. Pan et al., "Magnetic resonance imaging markers of cerebral small vessel disease in hematoma expansion of intracerebral hemorrhage," *Journal of Stroke and Cerebrovascular Diseases*, vol. 27, no. 7, pp. 2006–2013, 2018.

[42] C. Zeng, F. Lin, P. Ge, D. Zhang, S. Wang, and J. Zhao, "Homocysteine level and risk of hemorrhage in brain arteriovenous malformations," *Disease Markers*, vol. 2021, Article ID 8862299, 9 pages, 2021.

[43] Z. Li, L. Sun, H. Zhang et al., "Elevated plasma homocysteine was associated with hemorrhagic and ischemic stroke, but methylenetetrahydrofolate reductase gene C677T polymorphism was a risk factor for thrombotic stroke: a multicenter case-control study in China," *Stroke*, vol. 34, no. 9, pp. 2085–2090, 2003.

[44] W. Zhao, F. Gao, L. Lv, and X. Chen, "The interaction of hypertension and homocysteine increases the risk of mortality among middle-aged and older population in the United States," *Journal of Hypertension*, vol. 40, no. 2, pp. 254–263, 2022.